Applied Catalysis B: Environmental 187 (2016) 218–227

Contents lists available at ScienceDirect

Applied Catalysis B: Environmental

journal homepage: www.elsevier.com/locate/apcatb

N_2O decomposition on CoO_x, CuO_x, FeO_x or MnO_x supported on ZrO_2: The effect of zirconia doping with sulfates or K^+ on catalytic activity

Daniela Pietrogiacomi[a,b,*], Maria Cristina Campa[b], Lea Roberta Carbone[a], Simonetta Tuti[c], Manlio Occhiuzzi[a,b]

[a] Dipartimento di Chimica, "Sapienza" Università di Roma, Piazzale Aldo Moro 5, 00185 Roma, Italy
[b] CNR-Istituto per lo Studio dei Materiali Nanostrutturati, c/o Dipartimento di Chimica, "Sapienza" Università di Roma, Piazzale Aldo Moro 5, 00185 Roma, Italy
[c] Dipartimento di Scienze, Università degli studi "Roma Tre", Via della Vasca Navale 79, 00146 Roma, Italy

ARTICLE INFO

Article history:
Received 26 October 2015
Received in revised form
28 December 2015
Accepted 9 January 2016
Available online 14 January 2016

Dedicated to Professor Alessandro Cimino on the occasion of his 90th birthday in 2016.

Keywords:
N_2O decomposition
Transition metal oxide supported on ZrO_2
Sulfated-ZrO_2
Alkali-doped ZrO_2

ABSTRACT

Zirconia doped with sulfates or K^+ were prepared by impregnation with $(NH_4)_2SO_4$, or KNO_3 aqueous solutions. MeO_x/ZrO_2 and MeO_x/doped-ZrO_2 catalysts (Me = Co, Cu, Fe or Mn) were prepared by wet impregnation of zirconia and doped-zirconia supports. The effect of doping on MeO_x properties was studied by XRD, UV–vis DRS, H_2-TPR and FTIR and the influence of doping on the catalytic activity for N_2O decomposition was investigated under ideal conditions (N_2O in He) and under *real* reaction conditions (addition of NO, O_2, and water vapour to the reactant mixture).

Characterization results indicated that all samples contained mainly dispersed Me^{n+} species interacting with the support. In MeO_x/sulfated-ZrO_2 the doping with electron-withdrawing sulfates stabilized the Me^{n+} oxidation state. In CoO_x/K-ZrO_2 samples the doping with electron-releasing K^+ increased the polynuclear CoO_x reducibility. FTIR characterization suggested that the electron-donor capacity of Co^{2+} site had the order CoO_x/sulfated-ZrO_2 < CoO_x/ZrO_2 < CoO_x/K-ZrO_2.

Catalytic results showed that dispersed Me^{n+} are the active site for N_2O decomposition on MeO_x/ZrO_2. The "twin peak pattern" of catalytic activity versus tmi d-electron number suggests that formation and stability of the intermediate $Me^{(n+1)+}O^-$ surface complex, requiring the mobility of Me^{n+} oxidation state, are key factors for activity. Because the electron-withdrawing sulfates lowered the electron-donor capacity of tmi, hindering the formation of $Me^{(n+1)+}O^-$, the effect of sulfate-doping was to decrease the *de*N_2O activity in MeO_x/sulfated-ZrO_2. Conversely, because the electron-releasing potassium cation increased electron-donor capacity of Co^{2+}, yielding an easier formation of the intermediate surface complex, the effect of K-doping was to increase the *de*N_2O activity in CoO_x/K-ZrO_2.

From an applied viewpoint, cobalt supported on ZrO_2 and K-doped ZrO_2 systems, that were affected by reversible inhibitory effect in *real* reaction conditions, are interesting catalysts for N_2O abatement and for simultaneous abatement of N_2O and NO with hydrocarbons.

1. Introduction

Nitrous oxide contributes to greenhouse effect with high global warming potential (about 300 times the GWP_{CO2}) and to stratospheric ozone depletion [1]. N_2O is produced in large amounts as a by-product from the manufacture of nitric and adipic acid as well as from industrial combustion processes. Considering its long atmospheric lifetime (about 150 years), the abatement of N_2O emission from industrial sources is necessary. Both catalytic decomposition and selective catalytic reduction become promising ways to abate this harmful greenhouse gas [2]. For industrial application the catalytic decomposition of nitrous oxide (*de*N_2O) is economic and produces no CO_2, although most of the active systems (metals, supported as well as unsupported pure and mixed oxides, and transition metal ions (tmi) in solid solution or exchanged in zeolites [3–6]) suffer deactivation in the presence of O_2, NO, H_2O in the reactant stream [2,7–9]. So far, in HNO_3 production plants, Fe-zeolite catalysts only show sufficient activity and stability [10,11].

As Fe-zeolite [12–14], also Co- [15,16] and Cu-zeolites [17] showed high activity for *de*N_2O, and the corresponding pure oxides (Fe_2O_3, Co_3O_4, CuO) yielded good activity at lower temperature

* Corresponding author at: Dipartimento di Chimica, "Sapienza" Università di Roma, Piazzale Aldo Moro 5, 00185 Roma, Italy.
E-mail address: daniela.pietrogiacomi@uniroma1.it (D. Pietrogiacomi).

http://dx.doi.org/10.1016/j.apcatb.2016.01.018
0926-3373/

[3,4,18]. When MeO_x is supported on ZrO_2 the tmi-support interaction improves catalytic performances. In fact CuO_x/, CoO_x/and FeO_x/ZrO_2 [3,19,20] had good *de*N_2O activity and, unlike zeolite-based systems, their catalytic activity was reversibly recovered when H_2O was eliminated from the feed gas [20]. For these systems we found that, when Me-content was below the limit up to the tmi were highly dispersed (2.0 for Co, 2.5 for Cu, and 2.8 for Fe atoms nm^{-2}), the turnover frequency (rate *per* site) for *de*N_2O did not depend on the metal content, suggesting that dispersed Co, Cu and Fe ions were the active sites [20]. The reaction pathway illustrated by a "localized approach" [21,22] proceeds through a surface complex between activated N_2O and active site. By consensus, N_2O decomposes by a redox step in which an electron transfer formed N_2 and an active surface oxygen species. For tmi-containing oxides active Me^{n+} acted as both electron-donor center, yielding $Me^{(n+1)+}O^-$ surface complex, and as electron-acceptor center to desorb dioxygen (cationic redox mechanism) [21,23,24]. For alkaline-earth oxides, not containing tmi [25,26], some specific surface O^{2-} activated N_2O, forming peroxide intermediates, whose migration/recombination restored surface O^{2-} by O_2 desorption (anionic redox mechanism).

In previous studies on the selective catalytic reduction of NO in MeO_x/ZrO_2 (Me = Co, Cu or Fe) we found that zirconia-doping with sulfates modified the redox properties and the dispersion of tmi, thus strongly affecting activity and selectivity [27–32]. Several studies on pure and mixed-oxide catalysts reported the effect of alkali-doping on their electronic properties and the improvement of their activity for *de*N_2O [26,33–37]. In this paper, for *de*N_2O we investigated the effect of doping with sulfates or with K^+ on the activity of pure zirconia matrix and on MeO_x supported catalysts (Me = Co, Cu, Fe or Mn). To clarify the role of tmi redox properties on the reactivity for *de*N_2O, we compared the activity of Me^{n+} dispersed on pure ZrO_2 and on doped ZrO_2 on samples with tmi-content near to the dispersion limit. MeO_x dispersion, Me^{n+} reducibility and reactivity were characterized by XRD, UV–vis DRS, H_2-TPR, FTIR and XPS. Because in tail-gas of nitric acid production, NO, O_2 and water vapour are always present, to obtain further insights on our catalyst performances, some selected catalysts have been investigated under addition of these gases into the reactant mixture (*real* reaction conditions).

2. Experimental

2.1. Sample preparation

The zirconia was prepared by hydrolysis of zirconium oxychloride with ammonia, as already described [38]. Before its use as a support, the material was dried at 383 K for 24 h and calcined at 823 K for 5 h. After calcination, the BET surface area of the ZrO_2 support (Z), measured by N_2 adsorption at 77 K, was 50 $m^2\,g^{-1}$. XRD spectra showed that Z was in the monoclinic phase.

MeO_x/ZrO_2 catalysts (Me/Z), with Me = Co, Cu, Fe or Mn, were obtained by impregnation of Z with aqueous solution of Me^{n+} salt ($Co(acetate)_2$, $Cu(nitrate)_2$, $Fe(nitrate)_3$ or $Mn(nitrate)_2$). Sulfated-zirconia were prepared by wet impregnation of Z with an aqueous $(NH_4)_2SO_4$ solution (SZ), or with an aqueous Na_2SO_4 solution (NaSZ), and by calcining at 823 K for 5 h. K-doped zirconia samples (KZ) were prepared by wet impregnation of Z with aqueous KNO_3 solutions with a nominal K amount of 1.0, KZ(1), or 4.0 atoms nm^{-2}, KZ(4), and by calcining at 823 K for 5 h. MeO_x/sulfated-ZrO_2 samples (Me/SZ) were obtained by impregnation of SZ with a toluene solution of acetylacetonate of Co^{2+}, Cu^{2+}, Fe^{3+} and Mn^{2+}. CoO_x/K-doped ZrO_2 (Co/KZ) was obtained by impregnation of KZ(1) with aqueous solutions of $Co(acetate)_2$. After impregnation, all samples were dried at 383 K and calcined at 823 K. Me-content was determined by atomic absorption (Varian SpectrAA-220). Sulfate content was determined on SZ and NaSZ by extraction of sulfates with NaOH 1.00 M, and ICP-MS (Varian Vista-Mpx) measurement of the resulting solution. All MeO_x/ZrO_2 and MeO_x/doped-ZrO_2 samples yielded BET surface area ($50 \pm 2\ m^2\,g^{-1}$) similar to that of zirconia support. Starting materials for catalyst preparation, catalyst name, analytical content of metal and sulfates are listed in Table 1.

As references, mechanical mixtures of ZrO_2 and MeO_x ($MeO_x = Co_3O_4$, CuO, Fe_2O_3 or Mn_2O_3) were prepared by grinding in an agate mortar an oxide amount equal to the analytical MeO_x-content of the corresponding supported MeO_x/ZrO_2 and used without further treatment. These samples were designated as Me-$Z_{(mix)}$.

2.2. Characterization measurements

XRD measurements were done with a Philips PW 1729 diffractometer (Cu Kα, Ni-filtered radiation) equipped with an IBM computer (software APD-Philips).

The UV–vis DRS spectra were recorded in air by using a Varian Cary 5E spectrometer equipped with a computer for data acquisition and analysis (software Cary Win UV).

H_2-TPR experiments were performed in a flow apparatus TPDRO 1100 Thermo Scientific. A fresh portion of sample (0.050–0.100 g), placed into a quartz reactor, was pretreated in a flow of 5% O_2/He mixture (20 cm^3 STP min^{-1}) at 793 K for 30 min, and then cooled in He to RT. H_2-TPR measurements were performed heating from RT up to 1223 K, with a ramp of 10 K min^{-1}, in a flow of 5% H_2/Ar mixture (10 cm^3 STP min^{-1}). Samples were maintained at the final temperature for 30 min. The H_2 consumption was detected by a TCD detector. Sulfate reduction products and water were trapped in a soda lime trap. To calibrate the H_2 consumption, a known amount of pure Ar was introduced into the flow of 5% H_2/Ar mixture (10 cm^3 STP min^{-1}). The reduction extent was evaluated from H_2 consumption and expressed as electron exchanged per metal atom (e/Me^{n+}) or sulfate ion (e/SO_4^{2-}).

FTIR spectra were recorded at RT by using a Perkin Elmer 2000 spectrometer equipped with an MCT detector, collecting 100 scans at a resolution of 4 cm^{-1}. Powdered materials were pelleted (pressure 1.5×10^4 kg cm^{-2}) in self-supporting disks of ca. 50 mg cm^{-2} and 0.1–0.2 mm thickness. All samples were placed into an IR quartz cell allowing thermal treatments *in vacuo* or in a controlled atmosphere. Before experiments, samples were activated by heating in O_2 from RT to 793 K, keeping at this temperature for 1 h, and evacuating thereafter at the same temperature for 1 h. Spectra after adsorption of gaseous probes are difference spectra obtained by subtracting to the collected spectrum that of the blank activated sample.

XPS spectra were collected by using an ESCALAB MkII (*VG Scientific*) spectrometer, equipped with a standard Al Kα excitation source and a 5-channeltron detection system. The spectra were collected at 50 eV constant pass energy. The value of binding energy (BE ± 0.2 eV) was calibrated by measuring the C 1s peak at BE = 285.0 eV. Spectroscopic data were processed by the CasaXPS v.2.2.84 software.

2.3. Catalytic experiments

The catalytic activity was measured in a flow apparatus at atmospheric pressure on 0.25 g of catalyst. Before each run, the catalyst was heated in flow of 2% O_2/He mixture (100 $cm^3\,min^{-1}$) at 773 K for 1 h. All catalysts were tested with N_2O feed (4000 ppm of in He). In some selected cases the catalysts were tested by adding 4000 ppm of O_2, 4000 ppm of NO, 2% H_2O separately or all together to the N_2O feed (*real* reaction conditions). The total flow rate was 50 $cm^3{}_{STP}/min^{-1}$ (space velocity 24,000 h^{-1}). Gas

Table 1
Catalysts and their main features.

Catalysts	Starting materials	Analytical content (ions nm^{-2})			H_2 consumption in TPR experiments (electrons/ion)	
		$[Me^{n+}]$	$[SO_4^{2-}]$	$[K^+]$	e/Me^{n+}	e/SO_4^{2-}
Z	ZrO_2					
SZ	$Z+(NH_4)_2SO_4$		3.1			7.2
NaSZ	$Z+Na_2SO_4$		2.0			7.1
KZ(1)	$Z+KNO_3$			1.0		
KZ(4)	$Z+KNO_3$			4.0		
Co/Z	$Z+Co(ac)_2$	2.2			2.4	
Co/SZ	$SZ+Co(acac)_2$	3.3	3.1			7.5[a]
Co(1)/KZ	$KZ(1)+Co(ac)_2$	0.9		1.0	2.2	
Co(2)/KZ	$KZ(1)+Co(ac)_2$	1.8		1.0		
Cu/Z	$Z+Cu(NO_3)_2$	2.5			2.2	
Cu/SZ	$SZ+Cu(acac)_2$	2.6	3.1		2.1	5.7
Fe/Z	$Z+Fe(NO_3)_3$	2.2			2.9	
Fe/SZ	$SZ+Fe(acac)_3$	2.2	3.1			6.2[a]
Mn/Z	$Z+Mn(NO_3)_2$	2.6			1.7	
Mn/SZ	$SZ+Mn(acac)_2$	2.3	3.1			5.8[a]

[a] Total hydrogen consumption to reduce both sulphates and Me^{n+} species.

mixtures were purchased from RIVOIRA and used without further purification. Reactants and products were analyzed by gas chromatography (Agilent 7890A GC system, equipped with two columns: (i) Molsieve 5A, for detecting O_2 and N_2; (ii) Porapack Q for detecting N_2O). On all catalysts the activity for *de*N_2O was stable with time on stream, throughout experiments lasting up to about 8 h.

Percent N_2O conversion and N_2O decomposition rate (R_{N_2O}/molecules s^{-1} g^{-1}) were calculated from N_2O molecules consumed or N_2 produced. R_{N_2O} were evaluated from experiments where 30% conversion was not exceeded. The turnover frequencies (N_{N_2O}/molecules s^{-1} Me^{-1}) were calculated as $N_{N_2O} = R_{N_2O}/[Me]$, where [Me] was the metal analytical concentration ([Me]/atom g^{-1}).

3. Results and discussion

3.1. Me^{n+} species: XRD, UV–vis DRS, and XPS characterization

XRD spectra of MeO_x/ZrO_2 and MeO_x/doped-ZrO_2 samples (not shown for brevity) showed reflections of monoclinic ZrO_2, indicating that segregated particles of MeO_x and $MeSO_4$, if present, were smaller than 5 nm.

DRS spectra of both Cu/Z and Cu/SZ samples (Fig. 1a) consisted of a broad band at 8000–19,000 cm^{-1}, due to dispersed Cu^{2+} in distorted octahedral sites [30,39,40]. Cu-$Z_{(mix)}$ showed a continuous absorption above 15,000 cm^{-1}, due to CuO [39]. The comparison of the spectra indicated that Cu/Z might contain small oxide amount, showing its spectrum a growing absorption above 15,000 cm^{-1}. In agreement with our previous work [30], the presence of sulfates favored the Cu^{2+} dispersion.

DRS spectra of Fe/Z, and Fe/SZ (Fig. 1b) were similar, consisting of very weak bands at about 21,000, 18,800 and 12,000 cm^{-1}, typical of Fe^{3+} complexes [31,41]. The spectrum of Fe-$Z_{(mix)}$ showed a continuous absorption starting at about 18,000 cm^{-1}, and bands at about 15,000 and 12,000 cm^{-1}, due to Fe_2O_3 oxide [42]. The comparison of the spectra suggests that both Fe/Z and Fe/SZ contained no Fe_2O_3.

DRS spectra of Mn/Z and Mn/SZ (Fig. 1c) consisted of a broad band at about 20,000 cm^{-1} with a shoulder at about 12,000 cm^{-1}. The absorption at about 20,000 cm^{-1} was consistent with Mn^{4+} [43,44], Mn^{3+}, and Mn^{2+}, the latter with very low extinction coefficient [45]. The shoulder at about 12,000 cm^{-1} was consistent with Mn^{3+} complexes and Mn_2O_3 (compare with Mn-$Z_{(mix)}$ spectrum).

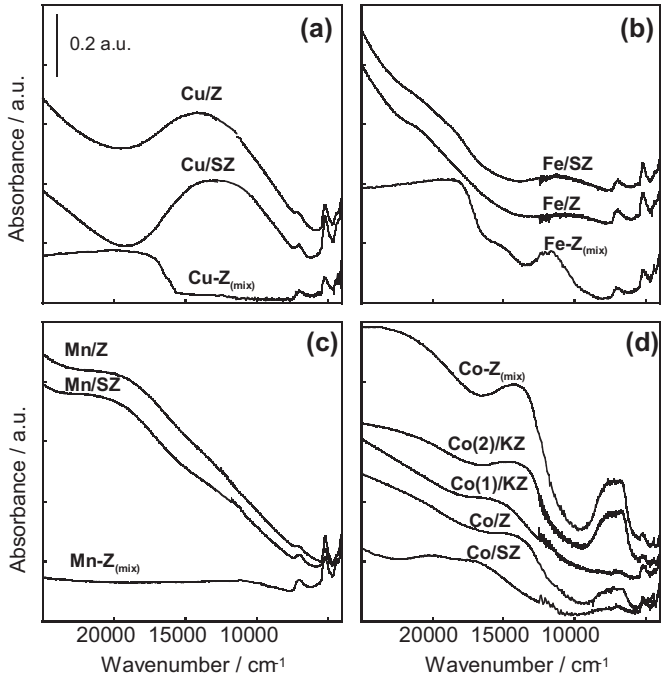

Fig. 1. UV–vis DRS spectra of MeO_x/ZrO_2 and relevant mechanical mixtures, MeO_x/sulfated-ZrO_2, and MeO_x/K-ZrO_2. Section (a) Cu/Z(2.5), Cu/SZ(2.6,3.1) and Cu-$Z_{(mix)}$. Section (b) Fe/Z(2.2), Fe/SZ(2.2,3.1) and Fe-$Z_{(mix)}$. Section (c) Mn/Z(2.6), Mn/SZ(2.3,3.1) and Mn-$Z_{(mix)}$. Section (d) Co/Z(2.2), Co/SZ(3.3,3.1), Co/KZ(0.9,1.0), Co/KZ(1.8,1.0), and Co-$Z_{(mix)}$. In parenthesis, Me and dopant analytical contents (atoms nm^{-2}) are specified, in that order.

We suggest in both Mn/Z and Mn/SZ the contemporary presence of Mn^{2+}, Mn^{3+} and Mn^{4+} and, possibly, of small amount of Mn_2O_3.

DRS spectrum of Co/SZ (Fig. 1d) showed weak absorptions of octahedral Co^{2+} (at about 19,900, 17,000, and 7300 cm^{-1}, [46]), whereas Co/Z spectrum showed weak absorptions at about 14,000 cm^{-1}, and at about 7500 cm^{-1}. Co-$Z_{(mix)}$ showed similar absorptions at about 14,000 cm^{-1}, and at about 7500 cm^{-1}, but with higher intensity, due to Co_3O_4 [27]. Co(1)/KZ spectrum showed the absorptions of octahedral Co^{2+} alone, whereas the Co(2)/KZ spectrum showed also bands of Co_3O_4. In Co/KZ, the K-doping favored Co_3O_4 formation, because the limit surface density shown by characterization to have high metal dispersion (2.0 atoms nm^{-2})

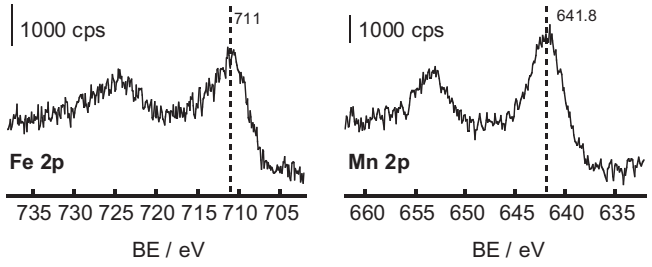

Fig. 2. XPS spectra of Fe/Z in the Fe 2p region and of Mn/Z in the Mn 2p region, as indicated.

lowered. On the contrary, in Co/SZ the sulfate-doping prevented oxide formation, in agreement with our previous papers [28].

As concerns the tmi-actual oxidation state, because DRS spectra of Fe/Z and Mn/Z were not conclusive we analyzed these samples by XPS. For Fe/Z (Fig. 2), the spectrum in the Fe 2p region showed a main $2p_{3/2}$ peak at 711.0 eV, typical of Fe^{3+}, with a weak tail at lower BE (about 709 eV) and a "shoulder" satellite at about 714 eV. Both the weak tail and the "shoulder" satellite peak are clear evidence of the existence of low amount of Fe^{2+} [47,48]. For Mn/Z (Fig. 2), the spectrum in the Mn 2p region showed a main $2p_{3/2}$ peak at 641.8 eV, typical of Mn^{3+}, having weak tails at higher and lower BE, due to Mn^{4+} and Mn^{2+} respectively [49]. Therefore, in Mn/Z Mn^{3+} was the predominant species with low amounts of Mn^{4+} and Mn^{2+}, respectively.

As concern tmi dispersion, in previous FTIR characterization of CuO_x/ZrO_2 [40], FeO_x/ZrO_2 [31], and CoO_x/ZrO_2 [28], we found that the intensity of tmi-nitrosyl band linearly increased with increasing metal content up to a limit value, indicating that up to this value tmi species were highly dispersed. In particular, copper species were dispersed up to 2.5, iron up to 2.8, and cobalt up to 2.0 atoms nm^{-2}. The dispersion limit values for copper and cobalt were also confirmed by XPS quantitative analysis [40]. In the present paper, Cu/Z, Fe/Z and Co/Z, prepared on the same support with the same method, yielded tmi-nitrosyl band whose intensity fall on the linear correlation within the experimental error (±5%, data not shown for brevity), suggesting good tmi dispersion.

On the whole, XRD, FTIR, and UV–vis DRS characterization suggested that Me/Z, Me/SZ and dilute Co/KZ samples contained mainly dispersed Me^{n+} species, interacting with the support. UV–vis DRS and XPS characterization indicated that Cu^{2+}, Fe^{3+} (with low amount of Fe^{2+}), Mn^{3+} (with low amounts of Mn^{4+} and Mn^{2+}), and Co^{2+} (with low amount of Co^{3+}) oxidation states were stabilized on ZrO_2.

3.2. Me^{n+} reducibility: H_2-TPR characterization

The pure zirconia matrix yielded negligible H_2 consumption up to 1223 K, indicating that no appreciable Zr^{4+} reduction occurred, in agreement with previous ESR results [50]. The H_2-TPR profiles of SZ and NaSZ matrices consisted of an intense peak at 923 K of H_2 consumption for the sulfate reduction, corresponding to $e/SO_4^{2-} \simeq 7$ (Table 1). This value suggests that sulfates reduced to SO_2 and/or S^{2-}, because reduction to H_2S corresponds to $e/SO_4^{2-} = 8$ [51]. In MeO_x/sulfated-ZrO_2 the H_2 consumption for sulfate reduction little decreased from 7 to about 6 e/SO_4^{2-} (Table 1), while the reduction temperature diminished to various extents depending on the supported MeO_x (from 90 K for Mn up to 200 K for Fe) (Fig. 3). These temperature decreases suggest that the tmi-support interaction caused a change in the sulfate-support one [51].

On Cu/Z (Fig. 4a) the H_2-TPR profile showed a stepwise reduction of dispersed Cu^{2+} species to Cu^+ and then to Cu° (composite peak at 473 K), and the reduction of CuO particles to Cu^0 (peak at 528 K)

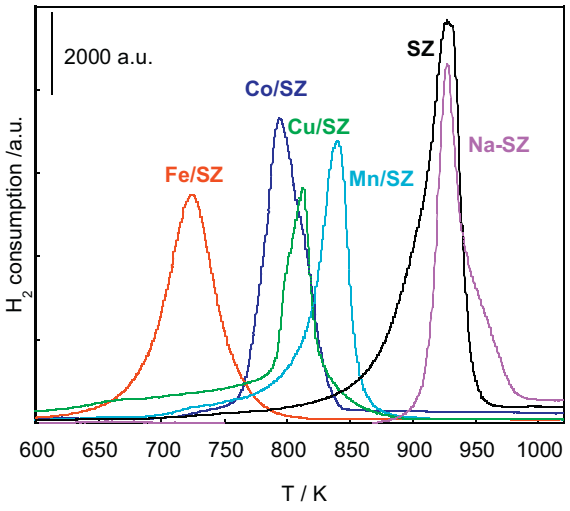

Fig. 3. H_2-TPR profiles of SZ, NaSZ, and MeO_x/SZ samples: H_2 consumption (a.u.) as a function of temperature (T/K).

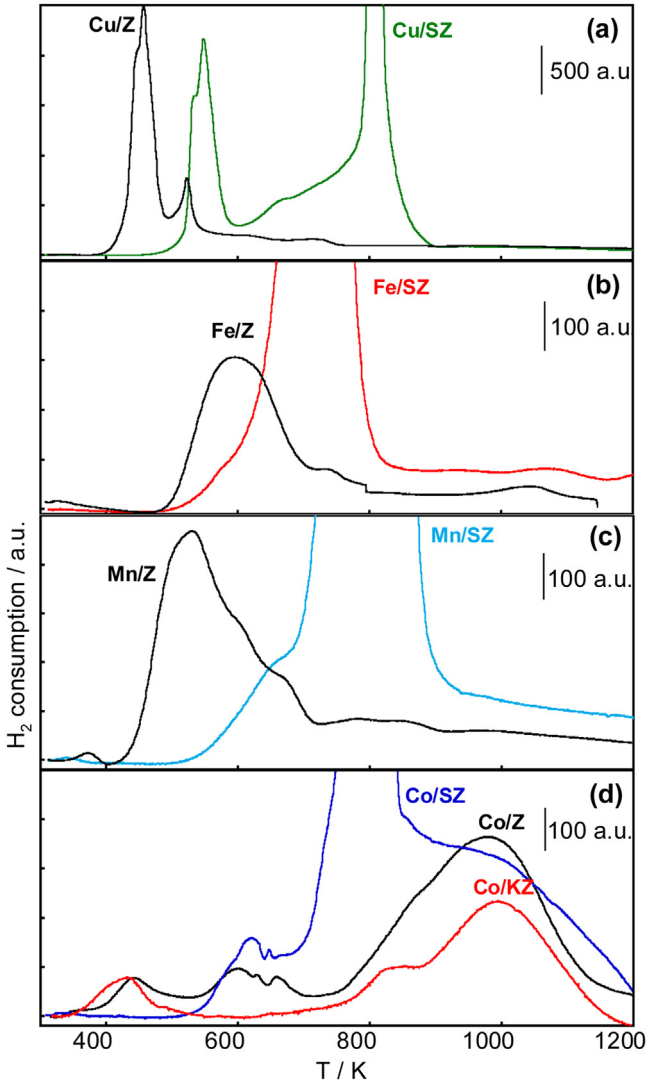

Fig. 4. H_2-TPR profiles of MeO_x/ZrO_2, and MeO_x/doped-ZrO_2: H_2 consumption (a.u.) as a function of temperature (T/K). Section (a) Cu/Z(2.5) and Cu/SZ(2.6,3.1). Section (b) Fe/Z(2.2) and Fe/SZ(2.2,3.1). Section (c) Mn/Z(2.6) and Mn/SZ(2.3,3.1). Section (d) Co/Z(2.2), Co/SZ(3.3,3.1) and Co/KZ(0.9,1.0). In parenthesis Me content and dopant analytical content (atoms nm^{-2}) are specified, in that order.

[19,52]. In agreement, the total H_2 consumption corresponded to about 2 e/Cu^{2+} (Table 1). The profile of Cu/SZ (Fig. 4a) showed (i) a $Cu^{2+} \rightarrow Cu^0$ reduction peak (e/Cu≃2.0), that occurred at higher temperature of about 75 K with respect to Cu/Z, and (ii) a sulfate reduction peak at about 813 K. Therefore, the presence of sulfates (i) raised Cu^{2+} reduction temperature and (ii) favored copper dispersion (no CuO reduction peak was detected), in agreement with UV–vis DRS results (Section 3.1). The growing profile of H_2 consumption in the range 600–773 K was due to H_2 spillover on metal copper that caused the reduction of a fraction of sulfate at lower temperature [53].

On Fe/Z (Fig. 4b) the H_2-TPR profile showed the $Fe^{3+} \rightarrow Fe^{2+}$ reduction (broad peak at about 590 K, e/Fe ≃1.0), occurring the $Fe^{2+} \rightarrow Fe^0$ reduction above 1173 K [54]. The profile of Fe/SZ showed the sulfate reduction alone (intense peak at about 773 K), that probably hid the Fe^{3+} reduction. Therefore, the reduction temperature of Fe^{3+} on Fe/SZ was higher than on Fe/Z, in agreement with previous results on similar samples [32].

On Mn/Z (Fig. 4c) the H_2-TPR profile showed an intense reduction peak at 523 K with shoulders at 608 and 673 K. The total hydrogen consumption was about 1.7 e/Mn. The main peak is assigned to the reduction of dispersed Mn^{n+} (n = 4 or 3) to Mn^{2+}, and the shoulders to the reduction of Mn_2O_3 to MnO [55]. Mn/SZ yielded an intense sulfate reduction peak at 838 K, with shoulders in the low temperature side, due to the reduction of dispersed Mn^{n+} (n = 4 or 3) to Mn^{2+}. The manganese reduction occurred at higher temperature than on Mn/Z.

On Co/Z (Fig. 4d) the H_2-TPR profile showed two weak peaks at 460 and 630 K, and a composite peak at higher temperature, 873–1038 K. In analogy with Co-zeolite [56,57], we assigned the peaks at 460 and 630 K to the reduction of poly-nuclear CoO_x species and of Co_3O_4 to metal respectively, and that above 873 K to the reduction of dispersed Co^{2+} to Co^0. The total H_2 consumption of Co/Z (e/Co = 2.4) confirms the presence of Co_3O_4 (Table 1). The H_2-TPR profile of Co/SZ showed a weak peak at about 580–670 K, the sulfate reduction peak at 798 K, and a broad peak above 850 K. Because on Co/SZ DRS detected no Co_3O_4, we assigned the peak at 580–670 K to the reduction of poly-nuclear CoO_x species that occurred at higher temperature than on Co/Z, due to sulfate-doping effect. The broad peak centered at about 1000 K was due to the reduction of dispersed Co^{2+}, and it occurred nearly at the same temperature as on Co/Z, because sulfates decomposed at lower temperature and did not influence the Co^{2+} reduction temperature. The profile of Co/KZ showed the reduction peak of poly-nuclear CoO_x species at lower temperature (about 20 K), and no reduction peak of Co_3O_4, in agreement with UV–vis DRS results (Section 3.1). The broad peak due to the reduction of dispersed Co^{2+} was similar to that of Co/Z.

On all Me/SZ, the effect of sulfate-doping was to decrease the Me^{n+} reducibility, and therefore to stabilize the Me^{n+} oxidation state, in agreement with previous FTIR results [27–29,31,32]. Conversely, on Co/KZ the effect of K-doping was to increase the poly-nuclear CoO_x reducibility. On alkali-promoted Co_3O_4 a similar effect was found [36,58].

3.3. Catalytic activity for N_2O decomposition

3.3.1. Pure and doped-ZrO_2

Pure ZrO_2 was active for N_2O decomposition above 673 K, yielding conversion equal to 32% at 773 K (Fig. 5). The SZ matrix showed conversions little lower than those of pure ZrO_2 (24% at 773 K), whereas NaSZ yielded conversions below 5% in the whole temperature range. The KZ catalysts yielded conversions lower than those of Z, decreasing the activity at increasing potassium content (N_2O conversion at 773 K 12% for KZ(1) and 5% for KZ(4)).

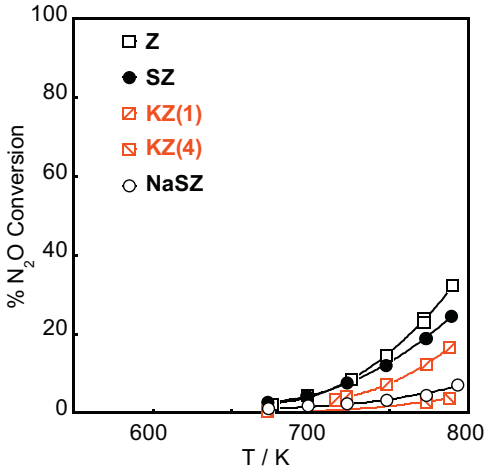

Fig. 5. N_2O decomposition on pure zirconia (Z), and on zirconia doped with sulfates (SZ and NaSZ) and with K^+ (KZ(1) and KZ(2)): percent N_2O conversion as a function of temperature. Catalysts as indicated.

Previous FTIR characterization indicated that in SZ covalent sulfates and di-sulfates anchored to surface Zr^{4+}, whereas in NaSZ ionic sulfates anchored [59]. Then, sulfates and their counter-ions (H^+ and Na^+) lowered the availability of surface O^{2-} for the gas phase. In KZ the alkaline cations covered surface oxygen anions. Taking into account these facts, the decrease of catalytic activity on doped samples indicated that surface O^{2-} were the active sites for N_2O dissociation via oxygen transfer, namely the "anionic redox mechanism" proposed for pure oxides [24,33,60]:

$$N_2O + O^{2-}{}_{surf} \rightarrow N_2 + O_2{}^{2-}{}_{surf} \quad (1)$$

This step was triggered by the compensation of the positive charge in the middle nitrogen atom of N_2O with the negative charge on the $O^{2-}{}_{surf}$ ion [24].

In NaSZ and KZ(4) the complete unavailability of active surface O^{2-} accounts for their inactivity, whereas in KZ(1.0) the partial coverage of O^{2-} by K^+ accounts for its partial activity. Although the coverage of surface O^{2-} was high in SZ, its activity may be ascribed to the bridged oxygen of di-sulfates, suitable to form peroxide.

The second reaction step concerns oxygen desorption [22], with the migration/recombination of oxygen ions via Langmuir–Hinshelwood (L-H) mechanism:

$$O_2{}^{2-}{}_{surf} + O_2{}^{2-}{}_{surf} \rightarrow 2O^{2-}{}_{surf} + O_2 \quad (2)$$

or via Eley–Rideal (E-R) mechanism:

$$N_2O + O_2{}^{2-}{}_{surf} \rightarrow N_2 + O_2 + O^{2-}{}_{surf} \quad (3)$$

3.3.2. MeO_x/ZrO_2

For the *de*N_2O, MeO_x/ZrO_2 (Me = Co, Cu, Fe or Mn) catalysts in the temperature range 573–773 K were more active than pure ZrO_2 (Fig. 6). This result agrees with that we found in a previous paper on N_2O decomposition [20], namely that Co, Cu and Fe isolated on ZrO_2 were the active sites, with an activity order Co > Cu > Fe. The results of this paper indicates that, as Co, Cu and Fe, dispersed Mn ions were active sites for N_2O decomposition, showing an activity in between those of Cu/Z and Fe/Z.

On diluted tmi MgO-based solid solutions Cimino and Stone [22] found that (i) isolated tmi were active for the *de*N_2O, and (ii) the activity of isolated species, that had a standardized coordination with oxide ions, could be considered as a function of their d-configuration. They plotted the "absolute" rate constant (k_{abs}/m s^{-1} ion^{-1}) as a function of the tmi d-electron number in calcined solid solution, and they found a twin-peak activity pattern.

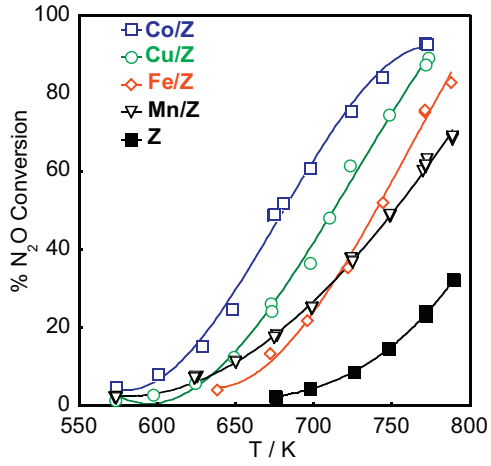

Fig. 6. N_2O decomposition on MeO_x/ZrO_2 (Me = Co, Cu, Fe or Mn): percent N_2O conversion as a function of temperature. Catalysts as indicated.

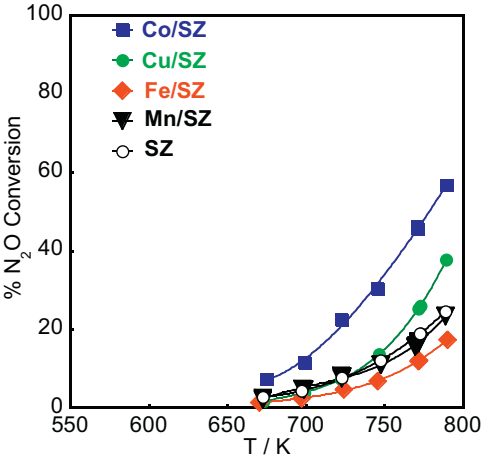

Fig. 8. N_2O decomposition on MeO_x/sulfated-ZrO_2 (Me = Co, Cu, Fe or Mn): percent N_2O conversion as a function of temperature. Catalysts as indicated.

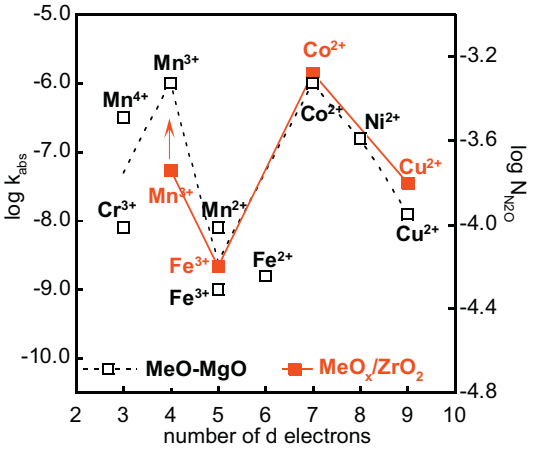

Fig. 7. The activity for N_2O decomposition at 625 K of dispersed Me^{n+} in MeO_x/ZrO_2 and in MeO_x-MgO solid solution as a function of d-electron number. The activity was expressed as turnover frequencies (N_{N_2O}/molecules s^{-1} Co^{-1}) for MeO_x/ZrO_2 and as absolute rate constant (k_{abs}/m s^{-1} ion^{-1}) for MeO-MgO with Me at 1 mol% concentration. The values for MeO_x-MgO solid solution were from Ref. [22].

This "d-correlation" indicated that a localized interaction between reactant and surface was implicated, because the crystal field stabilization energy (CFSE) of the tmi surface complex influenced the catalytic activity [22,61]. For our MeO_x/ZrO_2, because Cu^{2+}, Fe^{3+}, Co^{2+} and Mn^{3+} species were dispersed (see Section 3.1), we hypothesized that after calcination the exposed tmi had a standardized coordination with oxide ions. Therefore, we plotted the turnover frequency (N_{N_2O}/molecules s^{-1} ion^{-1}) of MeO_x/ZrO_2 as a function of d-configuration. The N_{N_2O} measured in our flow apparatus is analogous to the "absolute" rate constant measured in the static apparatus used for solid-solutions. A similar twin peak pattern was found for both solid solutions and supported ZrO_2 system (Fig. 7). In Mn/Z, that contained mainly Mn^{3+} (XPS evidence), we attribute the N_{N2O} value to the Mn^{3+} d^4-configuration. Because Mn/Z contained also minor amount of Mn^{4+} and Mn^{2+}, that in solid solutions were less active than Mn^{3+} [62], the plotted N_{N_2O} value, calculated assuming all Mn as active sites, was a lower limit. The similarity of the catalytic behavior of tmi in MgO solid solutions and in supported zirconia systems suggests that, as the tmi isolated in the solid solution surface, the tmi dispersed in the out-layer of ZrO_2 formed a surface complex with oxide ligands having a specific CFSE. This finding suggests a strong interaction of Me^{n+} with zirconia surface in agreement with previous ESR characterization on CuO_x/ZrO_2 system [40], evidencing the 5- or 6-coordination of supported Cu^{2+}.

The d-correlation found for MeO_x/ZrO_2 indicated that the "cationic redox mechanism" operated in *de*N_2O, namely tmi acted as electron-donor center toward the anti-bonding orbital of N_2O [22,24]

$$N_2O + Me^{n+} \leftrightarrows Me^{(n+\delta)+}N_2O^{\delta-}{}_{ads} \quad (4a)$$

$$Me^{(n+\delta)+}N_2O^{\delta-}{}_{ads} \rightarrow N_2 + Me^{(n+1)+}O^{-}{}_{ads} \quad (4b)$$

The second step consists in tmi reduction for oxygen desorption, via E-R mechanism:

$$Me^{(n+1)+}O^{-}{}_{ads} + N_2O \rightarrow N_2 + O_2 + Me^{n+} \quad (5)$$

or via L-H mechanism, with the migration/recombination of oxygen ions, requiring nearby adsorption sites:

$$Me^{(n+1)+}O^{-}{}_{ads} + Me^{(n+1)+}O^{-}{}_{ads} \leftrightarrows O_2 + 2Me^{n+} \quad (6)$$

Therefore, the formation and the stability of the $Me^{(n+1)+}O^{-}{}_{ads}$ surface complex are crucial for the activity. The key factor for the decomposition in any case is the aptitude of tmi to change its oxidation state. The redox couple reported in the literature are Co^{2+}/Co^{3+} [3], Cu^{+}/Cu^{2+} [63], Mn^{3+}/Mn^{4+} [62], and Fe^{2+}/Fe^{3+} [3]. The initial oxidation state of Cu^{2+} and Fe^{3+} surface ions can be reduced by the activation treatment or by the first dose of N_2O, that abstracts the labile O^{2-} ions on the surface. In agreement, our TPR characterization showed the Cu^{2+}, Mn^{n+} with n = 3 or 4, and Fe^{3+} on ZrO_2 easily reduced to Cu^{+}, Mn^{2+}, and Fe^{2+}, whereas Co^{2+} did not reduce.

Taking into account that in a previous paper [20] we found that isolated tmi were active and that the oxygen desorption via L-H needs nearby active sites, we infer that in our samples, which contain isolated tmi, the O_2 desorption mainly occurred via E-R (step 5) even if recombination via L-H (step 6) cannot be excluded.

3.3.3. *MeO_x/doped-ZrO_2*

Whereas in SZ the sulfate-doping yielded negligible change of catalytic activity (Fig. 5), the doping of MeO_x/ZrO_2 caused a marked activity decrease. Each Me/SZ showed N_2O conversion markedly lower than those of the corresponding Me/Z sample in the whole temperature range (compare Fig. 6 with Fig. 8). The activity of Cu/SZ, Fe/SZ and Mn/SZ was similar to that of the SZ matrix, suggesting that the anionic redox mechanism of the matrix was probably competitive. Co/SZ alone showed a significant tmi activity. In pure tmi-oxides the alkali-doping improved the *de*N_2O activity [35,36]. Therefore, we investigated the effect of K-doping on Co/KZ, comparing its catalytic activity with that of Co/Z and of Co/SZ. Considering

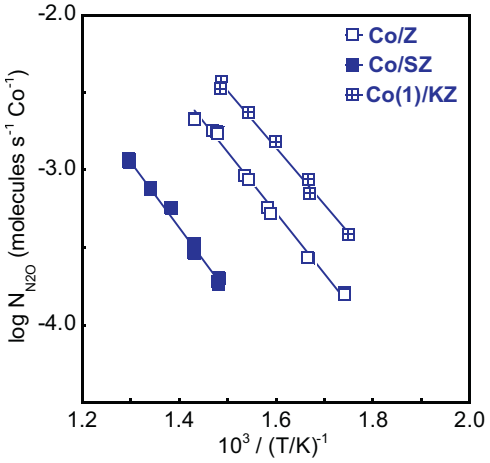

Fig. 9. Arrhenius plot for N_2O decomposition on CoO_x/ZrO_2, CoO_x/sulfated-ZrO_2 and CoO_x/K-ZrO_2 catalysts, as indicated: log N_{N_2O} *vs.* 1/T (N_{N_2O}/molecules s^{-1} $atom^{-1}$).

that Co/KZ (1.8,1.0) contained a non-negligible amount of Co_3O_4, we studied Co/KZ(0.9,1.0) containing dispersed Co^{2+} species alone. This sample yielded in the whole temperature range N_2O conversion values similar to those of Co/Z(2.2) (Figure not shown for brevity). Because the K-doped sample contained a lower cobalt amount than Co/Z and Co/SZ, the comparison of samples activity can be inferred by turnover frequency (N_{N2O}/molecules s^{-1} Co^{-1}), being activation energy values quite similar (75 ± 5 kJ mol^{-1}) and assuming that all cobalt ions or a constant fraction of them were active sites. The activity order for *de*N_2O was Co/KZ>Co/Z≫Co/SZ (Fig. 9).

3.4. *Effect of ZrO_2 doping on Me^{n+} reactivity: FTIR characterization*

In our previous papers [27–29,31,32], FTIR characterization showed that Me^{n+} (Co^{2+}, Cu^{2+}, or Fe^{3+}) in MeO_x/sulfated-ZrO_2 samples had lower reducibility and higher Lewis acid strength than in MeO_x/ZrO_2. We ascribed these effects to the electron withdrawing properties of the sulfate anchored to the ZrO_2 surface. In the present paper, in Co-containing samples, by using CO, NO and N_2O as probe molecules, we compared the effect on surface site of ZrO_2-doping with sulfates with that of ZrO_2-doping with K^+.

CO adsorption on Co/Z (Fig. 10) yielded, in addition to small amount of Zr^{4+}-carbonyls (2190–80 cm^{-1}) and carbonates (1650–1000 cm^{-1}, not shown), σ-coordinated Co^{2+}-CO (2150 cm^{-1}), weak σ-coordinated Co^{3+}-CO (2185 cm^{-1}) and π-coordinated linear and bridged Co^{n+}-carbonyls ($0 \leq n<2$) (2130–1700 cm^{-1}) [27]. These complex spectra indicated a high surface heterogeneity. On Co/SZ (Fig. 10) CO adsorption yielded a single intense band of Co^{2+}-CO, indicating a decrease of site heterogeneity. The Co^{2+}-CO band occurred at a higher wavenumber (about 2200 cm^{-1}) than on Co/Z. This blue-shift, due to an increase of σ-donation from CO to tmi, indicated an increase of Co^{2+} Lewis acid strength. Moreover, on Co/SZ no carbonates were detected, indicating no Co^{2+} reduction. Therefore, the presence of sulfates induced a decrease of the electron-density on Co^{2+} sites and the stabilization of the Co^{2+} oxidation state [28]. Co/KZ (Fig. 10) showed bands similar to those detected on Co/Z, but all occurring at lower wavenumber. The red-shift for Co^{2+}—CO and Co^{3+}—CO bands was ascribed to a lower Lewis acid strength of cobalt sites (decreasing the σ-donation from CO to tmi), and for Co^{n+}-carbonyls ($0 \leq n<2$) to a higher electron-donor capacity of the reduced cobalt sites (increasing the back π-donation from Co^{n+} to CO).

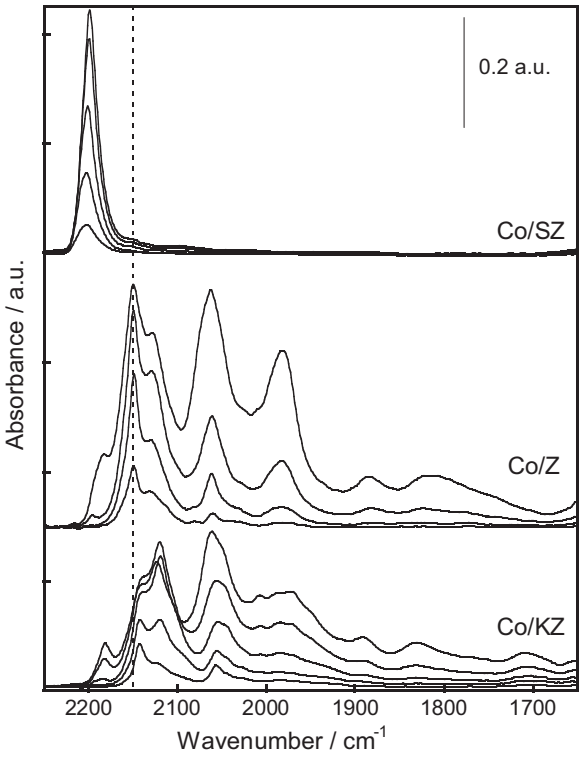

Fig. 10. FTIR spectra of CO adsorbed at RT on $CoOx/ZrO_2$, CoO_x/sulfated-ZrO_2, and CoO_x/K-ZrO_2 at increasing equilibrium pressure up to 30 Torr.

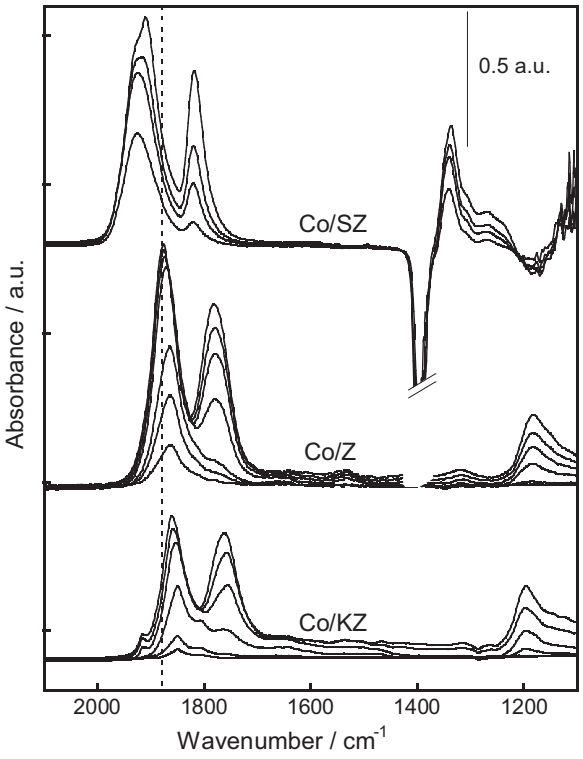

Fig. 11. FTIR spectra of NO adsorbed at RT on $CoOx/ZrO_2$, CoO_x/sulfated-ZrO_2, and CoO_x/K-ZrO_2 at increasing equilibrium pressure up to 30 Torr.

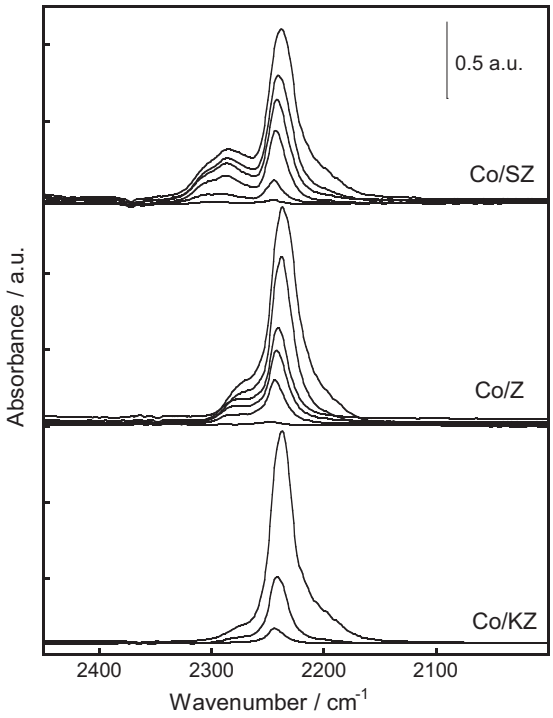

Fig. 12. FTIR spectra of N_2O adsorbed at RT on $CoOx/ZrO_2$, CoO_x/sulfated-ZrO_2, and CoO_x/K-ZrO_2 at increasing equilibrium pressure up to 70 Torr.

NO adsorption on all Co-containing samples, (Fig. 11) yielded bans of Co^{2+}-nitrosyl and -dinitrosyl (in the 2000–1700 cm^{-1} region), and of nitro, nitrites and/or nitrates compounds (NO_y in the 1500–900 cm^{-1} region) [27,28,64]. On Co/SZ, the negative peak at about 1400 cm^{-1} and the positive absorption at lower wavenumbers (1350–1200 cm^{-1} region) arose from the $\nu_{S=O}$ red-shift, because of side interactions of surface sulfates with adjacent irreversibly adsorbed NO_y species [28]. Compared to Co/Z, on Co/SZ the Co^{2+}-nitrosyl and -dinitrosyl bands (i) sharpened, indicating a lower heterogeneity of Co^{2+} sites, and (ii) shifted to higher wavenumber, indicating a higher Lewis acid strength of Co^{2+} in the presence of electron-withdrawing sulfates [28]. Conversely, on Co/KZ Co^{2+}-nitrosyl bands shifted to lower wavenumber than on Co/Z, because of an increase of π-donation in nitrosyls, indicating a lower Lewis acid strength of Co^{2+} sites in the presence of electron-releasing K^+. The K-doping implied also an increased basicity of oxidic ions, that accounted for the highest amount of adsorbed NO_y species on Co/KZ.

N_2O adsorption on all Co-containing samples (Fig. 12) showed an intense band at 2245 cm^{-1}, due to N_2O bonded via O-atom to Lewis acid sites, and a broad shoulder at about 2270–2310 cm^{-1}, due to N_2O bonded via N-atom to Lewis acid site with higher strength [64]. Comparing Co/Z with the doped samples, the amount of this latter species followed the order Co/SZ>Co/Z>Co/KZ.

On the whole, FTIR characterization by CO, NO or N_2O showed the same Co^{2+} Lewis acid strength order: Co/SZ>Co/Z>Co/KZ. Thus, the electron density at the cobalt site had an inverse order. In agreement, a close parallelism was found in our laboratory between acid-base properties and electron donor activity for surface sites of oxides [65]. Consequently, in Co/KZ, having higher Co^{2+} electron-density, the electron-donor capacity of Co^{2+} toward N_2O was higher and thus the formation of $Co^{3+}O^-_{ads}$ surface complex was easier (step 1a and b, Section 3.2.2). This finding accounts for its higher activity for *de*N_2O.

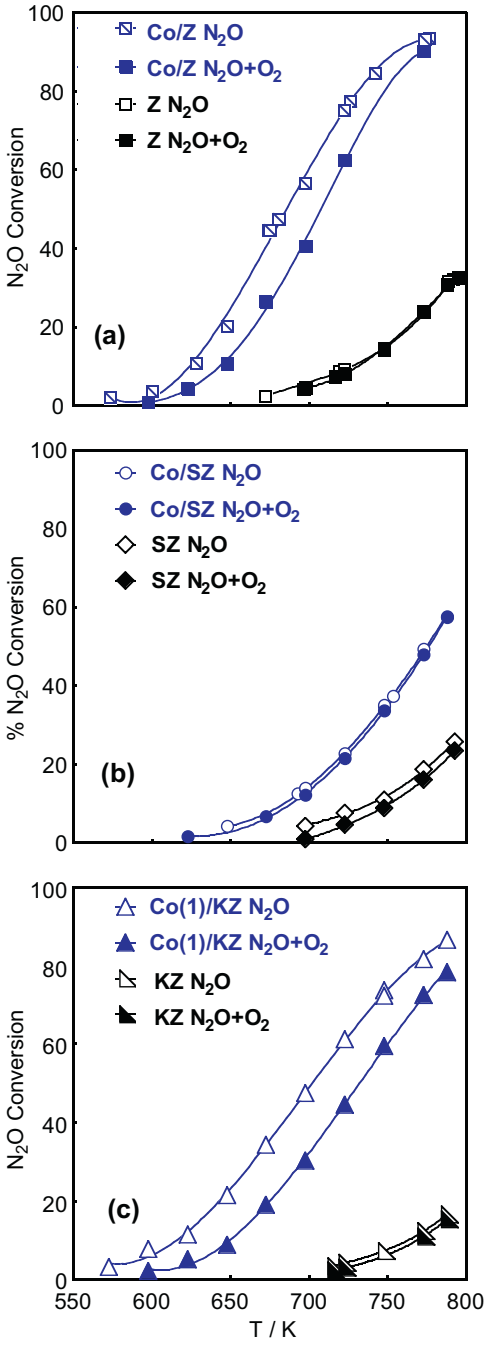

Fig. 13. Dependence of N_2O conversion on the O_2 addition in the reactant mixtures: percent N_2O conversion as a function of temperature. Section (a) Co/Z and Z. Section (b) Co/SZ and SZ. Section (c) Co(1)/KZ and KZ(1).

3.5. The dependence of catalytic activity on O_2 addition

Because the interaction of molecular oxygen with the surface gives information on the reaction mechanism, we investigated the effect of O_2 addition to the reaction stream on N_2O conversion. On ZrO_2, doped-ZrO_2 and Co/SZ the addition of 2% O_2 left N_2O conversion unchanged, whereas on Co/Z and on Co/KZ it caused a conversion decrease (Fig. 13).

In ZrO_2 and doped-ZrO_2 the absence of reaction inhibition by O_2 suggests that either the active electron-donor center ($O^{2-}{}_{surf}$) adsorbed no O_2 or the O_2 desorption occurred via the E-R mechanism, that did not depend on O_2 pressure, in agreement with Kapteijn [3].

In Co/Z and Co/KZ, on which we proposed a O_2 desorption via E-R step, the O_2 inhibition can be accomplished (i) via a two steps mechanism yielding $Co^{3+}O_2^-$ adduct intermediate and depending on O_2 pressure:

$$Co^{3+}O^- + N_2O \rightarrow Co^{3+}O_2^- + N_2 \rightarrow O_2 + Co^{2+}$$

as suggested for Co-ZSM5 [15], or (ii) via the competitive oxygen adsorption on Co^{2+}, leading to a decrease of the working active site amount in step 1 (Section 3.3.2). Others have already described the formation of cobalt superoxide $Co^{3+}O_2^-$ with O_2 or with N_2O on other matrices [66–70]. The higher O_2 inhibition in Co/KZ than in Co/Z (Fig. 13a and c) can be explained by the enhanced electron-donor properties of surface Co^{2+}, due to electron-releasing K^+ that favored both the formation of $Co^{3+}O_2^-$ adduct and the competitive O_2 adsorption. The absence of O_2 inhibition on Co/SZ (Fig. 13b) can be explained by the lower electron-donor properties of surface Co^{2+}, due to electron-withdrawing sulfates or by the occurrence of H.-R. desorption mechanism.

3.6. CoO_x/ZrO_2 and CoO_x/doped-ZrO_2 under real reaction conditions

To investigate the performance of Co-containing catalysts in *real* reaction conditions, NO, O_2 and water vapour, both separately and all together, were added into the reactant mixture. The addition effect on N_2O conversion (Fig. 14) was investigated at 773 K and reported as normalized N_2O conversion (conversion after addition/conversion before addition).

The addition of O_2 caused an activity decrease higher on Co/KZ than on Co/Z, whereas it had no effect on Co/SZ (see Section 3.5). On all Co-containing catalysts the addition of NO yielded negligible effect on the activity, whereas the addition of H_2O had a significant effect, possibly due to water adsorption on Co active sites. On Co/SZ this decrease was markedly higher than on Co/Z and Co/KZ, possibly due to both water adsorption and dis-anchorage of active di-sulfate species.

On Co/Z and Co/KZ the addition of NO + O_2 to the N_2O + H_2O mixture (*real* reaction conditions) caused a higher decrease of activity than that caused by the addition of water alone, due to the coverage of active sites by NO_y. The decrease of activity was higher on Co/KZ than on Co/Z, possibly because the stability of adsorbed NO_y on Co/KZ, due to the higher basicity of the adsorption sites, was higher than on Co/Z. Conversely, on Co/SZ in *real* conditions the activity did not decrease, possibly because no NO_y species adsorbed.

On all catalysts, (i) the activity after every gas addition was stable as a function of time on stream up to 120 min, and (ii) a subsequent treatment in He at 773 K completely restored the activity (2nd N_2O in Fig. 14), confirming that the activity decrease was due to reversible adsorption phenomena. On the contrary, analogous treatment on zeolites failed to restore the activity [8], because zeolite exposure to H_2O at the reaction temperature may irreversibly de-aluminate or segregate metal oxide.

4. Conclusions

On CoO_x, CuO_x, FeO_x or MnO_x supported on ZrO_2, isolated metal ions are active for N_2O decomposition. The tmi dispersion indicates the strong interaction of MeO_x with ZrO_2 support. The "twin peak pattern" of catalytic activity as a function of tmi d-electron number, found on these catalysts as on the corresponding solid solutions, confirmed that active Me^{n+} decomposed N_2O via cationic redox mechanism. The formation and stability of $Me^{(n+1)+}O^-$ surface complex, requiring the mobility of Me^{n+}-oxidation state, are key factors for activity. The effect of zirconia-doping with sulfates or K^+ was to change in an opposite way the mobility of Me^{n+} oxidation state.

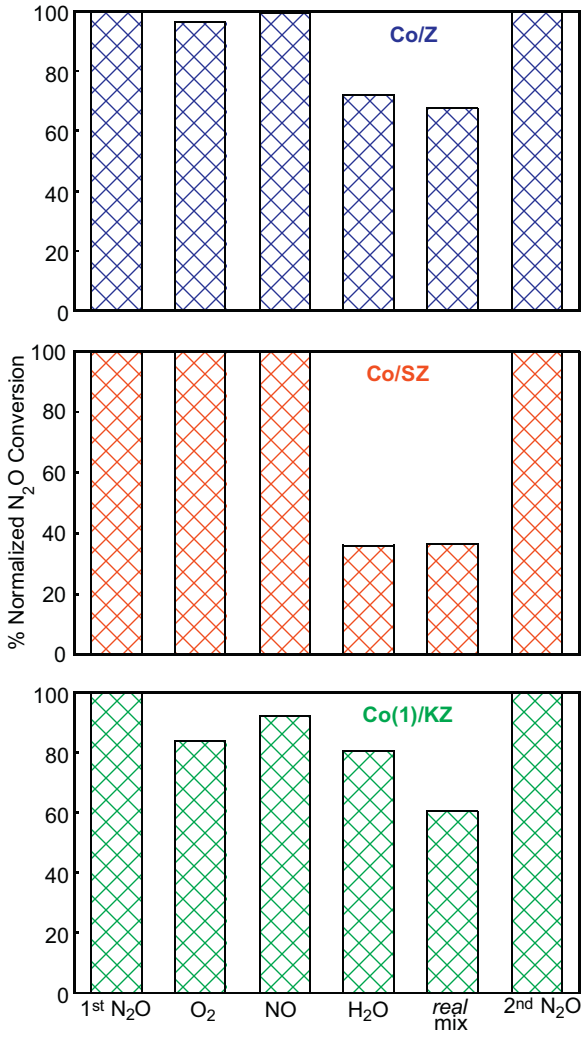

Fig. 14. The *de*N_2O activity of Co-containing samples in *real* reaction conditions. Normalized N_2O conversion at 773 K on activated samples (1st N_2O), after addition to the feed of O_2, NO, H_2O separately (as specified) or all together (*real* mix), and on samples re-activated after each gas-addition (2nd N_2O). N_2O conversion was normalized as (conversion after addition/conversion before addition). Catalysts as indicated.

Electron-withdrawing sulfates caused in MeO_x/sulfated-ZrO_2 the decrease of the electron-donor capacity of supported tmi (H_2-TPR and FTIR evidence). Consequently, because the formation of $Me^{(n+1)+}O^-$ surface complex was hindered, the *de*N_2O activity decreased. With the exception of CoO_x/sulfated-ZrO_2, the activity decreased down to the level of sulfated-ZrO_2 matrix, where the O^{2-} surface species were the active sites via anionic redox mechanism.

Conversely, electron-releasing K^+ caused in CoO_x/K-ZrO_2 the increase of the electron-donor capacity of supported Co^{2+} species (FTIR evidence). This effect induced (i) the easier formation of $Co^{3+}O^-$ surface complex, accounting for the higher activity for the *de*N_2O of Co^{2+} site, and (ii) the competitive phenomena of oxygen adsorption, causing the activity inhibition by gaseous O_2.

Because tmi and K^+ compete for the same anchoring sites, K-doping lowered the limit dispersion value for Co^{2+} on ZrO_2. The K-doped sample performances for *de*N_2O could be improved by the use of ZrO_2 support with higher surface area, as tetragonal zirconia.

From an applied viewpoint, CoO_x/ZrO_2 and CoO_x/K-ZrO_2 systems, that in *real* reaction conditions were partially and reversibly deactivated, are interesting catalysts for N_2O abatement. Being CoO_x/ZrO_2 catalyst also active for the selective catalytic reduction

of NO with C_3H_6, CoO_x/ZrO_2 and CoO_x/K-ZrO_2 catalysts are possible candidates for N_2O abatement and for simultaneous abatement of N_2O and NO with hydrocarbons.

Acknowledgements

We gratefully thank Dr. C. Tortolini for performing some catalyst preparations, Dr. A. Mezzi and S. Kaciulis for XPS measurements, and "Sapienza" University of Rome, Italy, for financial support.

References

[1] WMO, WMO Greenhouse Gas Bulletin, n.10, 6 November 2014.
[2] J. Pérez-Ramírez, F. Kapteijn, K. Schöffel, J.A. Moulijn, Appl. Catal. B 44 (2003) 117–151.
[3] F. Kapteijn, J. Rodriguez-Mirasol, J.A. Moulijn, Appl. Catal. B 9 (1996) 25–64.
[4] M. Konsolakis, ACS Catal. 5 (2015) 6397–6421.
[5] G. Grzybek, P. Stelmachowski, P. Indyka, M. Inger, M. Wilk, A. Kotarba, Z. Sojka, Catal. Today 257 (2015) 93–97.
[6] Y. Zhang, X. Wang, Y. Zhu, B. Hou, X. Yang, X. Liu, J. Wang, J. Li, T. Zhang, J. Phys. Chem. C 118 (2014) 1999–2010.
[7] T. Franken, R. Palkovits, Appl. Catal. B 176 (2015) 298–305.
[8] F. Kapteijn, G. Mul, G. Marbán, J. Rodriguez-Mirasol, J.A. Moulijn, in: J.W. Hightower, W.N. Delgass, E. Iglesia, A.T. Bell (Eds.), Studies in Surface Science and Catalysis, vol. 101, Elsevier Science Publ., Amsterdam, The Netherlands, 1996, p. 641.
[9] R.S. da Cruz, A.J.S. Mascarenhas, H.M.C. Andrade, Appl. Catal. B 18 (1998) 223–231.
[10] M. Schwefer, M. Groves, R. Siefert, R. Rainer, Patent EP 2286897 B1, (2003).
[11] Brochures of EnviNOx, are available at http://www.uhde.biz.
[12] B.R. Wood, J.A. Reimer, A.T. Bell, M.T. Janicke, K.C. Ott, J. Catal. 224 (2004) 148–155.
[13] E. Berrier, O. Ovsitser, E.V. Kondratenko, M. Schwidder, W. Grünert, A. Brückner, J. Catal. 249 (2007) 67–78.
[14] P. Sazama, N.K. Sathu, E. Tabor, B. Wichterlová, Š. Sklenák, Z. Sobalík, J. Catal. 299 (2013) 188–203.
[15] P.J. Smeets, Q. Meng, S. Corthals, H. Leeman, R.A. Schoonheydt, Appl. Catal. B 84 (2008) 505–513.
[16] M.C. Campa, V. Indovina, D. Pietrogiacomi, App. Catal. B 91 (2009) 347–354.
[17] P.J. Smeets, M.H. Groothaert, R.M. van Teeffelen, H. Leeman, E.J.M. Hensen, R.A. Schoonheydt, J. Catal. 245 (2007) 358–368.
[18] T. Goto, A. Niimi, K. Hirano, N. Takahata, S. Fujita, M. Shimokawabe, N. Takezawa, React. Kinet. Catal. Lett. 69 (2000) 375–378.
[19] Z. Liu, M.D. Amiridis, Y. Chen, J. Phys. Chem. B 109 (2005) 1251–1255.
[20] S. Tuti, F. Pepe, D. Pietrogiacomi, V. Indovina, React. Kinet. Catal. Lett. 72 (2001) 35–42.
[21] F.S. Stone, J. Solid State Chem. 12 (1975) 271–281.
[22] (a) A. Cimino, F.S. Stone, Adv. Catal. 47 (2002) 141–306;
(b) A. Cimino, F.S. Stone, in: G. Ertl, H. Knözinger, F. Schüth, J. Weitkamp (Eds.), Handbook of Heterogeneous Catalysis, 2nd edition, Wiley-VCH Verlag GmbH & Co. KGaA, Weinheim, 2008, pp. 1362–1373.
[23] Z. Sojka, M. Che, J. Phys. Chem. 100 (1996) 14776–14785.
[24] P. Pietrzyk, F. Zasada, W. Piskorz, A. Kotarba, Z. Sojka, Catal. Today 119 (2007) 219–227.
[25] E.J. Karlsen, M.A. Nygren, L.G.M. Pettersson, J. Phys. Chem. A 106 (2002) 7868–7875.
[26] L. Xue, H. He, C. Liu, C. Zhang, B. Zhang, Environ. Sci. Technol. 43 (2009) 890–895.
[27] D. Pietrogiacomi, S. Tuti, M.C. Campa, V. Indovina, Appl. Catal. B 28 (2000) 43–54.
[28] D. Pietrogiacomi, M.C. Campa, S. Tuti, V. Indovina, Appl. Catal. B 41 (2003) 301–312.
[29] D. Pietrogiacomi, D. Sannino, S. Tuti, P. Ciambelli, V. Indovina, M. Occhiuzzi, F. Pepe, Appl. Catal. B 21 (1999) 141–150.
[30] V. Indovina, D. Pietrogiacomi, M.C. Campa, Appl. Catal. B 39 (2002) 115–124.
[31] S. Tuti, F. Pepe, D. Pietrogiacomi, V. Indovina, Catal. Today 75 (2002) 373–378.
[32] V. Indovina, M.C. Campa, F. Pepe, D. Pietrogiacomi, S. Tuti, Appl. Catal. B 60 (2005) 23–31.
[33] W. Piskorz, F. Zasada, P. Stelmachowski, A. Kotarba, Z. Sojka, J. Phys. Chem. C 117 (2013) 18488–18501.
[34] H. Cheng, Y. Huang, A. Wang, L. Li, X. Wang, T. Zhang, Appl. Catal. B 89 (2009) 391–397.
[35] C. Ohnishi, K. Asano, S. Iwamoto, K. Chikama, M. Inoue, Catal. Today 120 (2007) 145–150.
[36] N. Pasha, N. Lingaiah, N. Seshu Babu, P. Siva Sankar Reddy, P.S. Sai Prasad, Catal. Commun. 10 (2008) 132–136.
[37] P. Stelmachowski, G. Maniak, A. Kotarba, Z. Sojka, Catal. Commun. 10 (2009) 1062–1065.
[38] A. Cimino, D. Cordischi, S. De Rossi, G. Ferraris, D. Gazzoli, V. Indovina, G. Minelli, M. Occhiuzzi, M. Valigi, J. Catal. 127 (1991) 744–760.
[39] H. Praliaud, S. Mikhailenko, Z. Chajar, M. Primet, Appl. Catal. B 16 (1998) 359–374.
[40] V. Indovina, M. Occhiuzzi, D. Pietrogiacomi, S. Tuti, J. Phys. Chem. B 103 (1999) 9967–9977.
[41] A.B.P. Lever, Inorganic Electron Spectroscopy, 2nd edition, Elsevier, Amsterdam, 1984 (p. 450, Table 6.13).
[42] S.J. Palmer, R.L. Frost, J. Mater. Sci. 44 (2009) 55–63.
[43] N. Li, A. Wang, Z. Liu, X. Wang, M. Zheng, Y. Huang, T. Zhang, Appl. Catal. B 62 (2006) 292–298.
[44] M. Occhiuzzi, D. Cordischi, R. Dragone, Phys. Chem. Chem. Phys. 5 (2003) 4938–4945.
[45] A.B.P. Lever, Inorganic Electron Spectroscopy, 2nd edition, Elsevier, Amsterdam, 1984, p. 435 (for Mn^{3+} complexes) and page 448 (for Mn^{2+} complexes).
[46] M. Che, F. Bozon-Verduraz, in: G. Ertl, H. Knözinger, J. Weitkamp (Eds.), Handbook of Heterogeneous Catalysis, vol. 2, Wiley, New York, 1997, p. 641.
[47] T. Yamashita, P. Hayes, Appl. Surf. Sci. 254 (2008) 2441–2449.
[48] Y. Okamoto, T. Kubota, Y. Ohto, S. Nasu, J. Catal. 192 (2000) 412–422.
[49] H.W. Nesbitt, D. Banerjee, Am. Mineral. 83 (1998) 305–315.
[50] M. Occhiuzzi, D. Cordischi, R. Dragone, J. Phys. Chem. B 106 (2002) 12464–12469.
[51] B.Q. Xu, W.M.H. Sachtler, J. Catal. 167 (1997) 224–233.
[52] G.X. Qi, X.M. Zheng, J.H. Fei, Z.Y. Hou, J. Mol. Catal. 176 (2001) 195–203.
[53] U. Schwabe, E. Bechtold, J. Catal. 26 (1972) 427–431.
[54] F.R. van den Berg, M.W.J. Crajé, A.M. van der Kraan, J.W. Geus, Appl. Catal. A 242 (2003) 403–416.
[55] D. Döbber, D. Kießling, W. Schmitz, G. Wendt, Appl. Catal. B 52 (2004) 135–143.
[56] X. Wang, H.-Y. Chen, W.M.H. Sachtler, Appl. Catal. B 26 (2000) L227–L239.
[57] C. Resini, T. Montanari, L. Nappi, G. Bagnasco, M. Turco, G. Busca, F. Bregani, M. Notaro, G. Rocchini, J. Catal. 214 (2003) 179–190.
[58] M. Haneda, Y. Kintaichi, N. Bion, H. Hamada, Appl. Catal. B 46 (2003) 473–482.
[59] D. Pietrogiacomi, D. Sannino, A. Magliano, P. Ciambelli, S. Tuti, V. Indovina, Appl. Catal. B 36 (2002) 217–230.
[60] P. Stelmachowski, F. Zasada, W. Piskorz, A. Kotarba, J.-F. Paul, Z. Sojka, Catal. Today 137 (2008) 423–428.
[61] A. Cimino, Chim. Ind. 56 (1974) 27–38.
[62] A. Cimino, V. Indovina, J. Catal. 17 (1970) 54–70.
[63] G. Centi, G. Cerrato, S. D'Angelo, U. Finardi, E. Giamello, C. Morterra, S. Perathoner, Catal. Today 27 (1996) 265–270.
[64] K.I. Hadjiivanov, Catal. Rev. Sci. Eng. 42 (2000) 71–144.
[65] D. Cordischi, V. Indovina, J. Chem. Soc. Faraday Trans. I 72 (1976) 2341–2347.
[66] El-M. El-Malki, D. Werst, P.E. Doan, W.M.H. Sachtler, J. Phys. Chem. B 104 (2000) 5924–5931.
[67] R.F. Howe, J.H. Lunsford, J. Am. Chem. Soc. 97 (1975) 5156–5159.
[68] V. Indovina, D. Cordischi, M. Occhiuzzi, A. Arieti, J. Chem. Soc. Faraday Trans. I 75 (1979) 2177–2187.
[69] D. Cordischi, V. Indovina, in: M. Che, G.C. Bond (Eds.), Adsorption and Catalysis on Oxide Surfaces, Elsevier Science Publ., Amsterdam, The Netherlands, 1985, pp. 209–220.
[70] E. Giamello, Z. Sojka, M. Che, A. Zecchina, J. Phys. Chem. 90 (1986) 6084–6091.